ELSEVIER

Tectonophysics 250 (1995) 31–46

TECTONOPHYSICS

A new estimate of the conditions for transition from basal ⟨a⟩ to prism [c] slip in naturally deformed quartz

Takamoto Okudaira [a,*], Toru Takeshita [a], Ikuo Hara [a], Jun-ichi Ando [b,1]

[a] *Department of Earth and Planetary Systems Science, Faculty of Science, Hiroshima University, Higashi-Hiroshima 739, Japan*
[b] *Department of Earth Science, Faculty of Science, Ehime University, Matsuyama 790, Japan*

Received 5 October 1994; accepted 27 March 1995

Abstract

Quartz *c*-axis fabrics of naturally deformed quartz in metacherts from the Ryoke metamorphic belt in the Yanai district, southwestern Japan, suggest that the prism [*c*], prism ⟨*a*⟩ and basal ⟨*a*⟩ slip systems were activated during the plastic deformation under high-temperature metamorphic conditions. With increasing temperature, quartz *c*-axis fabric patterns change from girdle type, through *X*-maximum with a faint crossed girdle, to *X*-maximum. The dominant orientation of subgrain boundaries in the quartz also changes from prism to basal with increasing temperature, closely correlated with the change in quartz *c*-axis fabric. The fabric transition is also accompanied by an abrupt increase of recrystallized quartz grain size. Moreover, observations with transmission electron microscopy (TEM) clearly identify the dominant activation of [*c*] slip through the presence of basal subgrain boundaries and free dislocations with the [0001] Burgers vector in the quartz from the metachert samples exhibiting *X*-maximum *c*-axis fabric. Based on these observations it is concluded that the mechanism switch from basal ⟨*a*⟩ to prism [*c*] slip systems occurred with increasing temperature in the metacherts. The transition temperature is petrologically estimated to be ca. 550–600°C at the natural strain rate.

1. Introduction

Quartz is one of the important minerals which constitute the upper continental crust. The mechanical behavior of the upper continental crust significantly depends on plastic deformation of quartz. The intracrystalline slip (dislocation glide) that operates during crystal-plastic deformation in minerals leads to the development of lattice preferred orientation (LPO) (referred to as fabric in this paper) in mineral aggregates. Although quartz grains deformed at relatively high-temperature conditions in the upper continental crust are in general entirely recrystallized, the *c*-axis fabric is essentially caused by intracrystalline slip. This conclusion is supported to a certain extent by the similarity between natural fabrics (e.g., Law et al., 1984) and simulated fabrics obtained using the Taylor model where fabric development results from intracrystalline slip alone (e.g., Lister et al., 1978). In contrast, the effect of dynamic recrystallization on fabric development could be indeed important at particular conditions (e.g., Gleason et al., 1993). However, the mechanisms of fabric devel-

* Corresponding author.
[1] Present address: Center for High Pressure Research and Department of Earth and Space Sciences, State University at Stony Brook, Stony Brook, NY 11794-2100, USA.

SSDI 0040-1951(95)00039-9

opment by dynamic recrystallization and the conditions where fabric development is controlled by dynamic recrystallization have not been fully understood yet.

There are several different families of slip systems in quartz and different families of slip systems dominate at different physical conditions and environments. The factors that determine the dominant slip systems include temperature (e.g., Tullis et al., 1973), P_{H_2O}(e.g., Griggs and Blacic, 1965; Linker et al., 1984), strain rate (e.g., Tullis et al., 1973), pressure (e.g., Kronenberg and Tullis, 1984) and defect chemistries (e.g., Hobbs, 1981, 1984). Among these parameters, temperature could be the most important factor to control the critical resolved shear stress (CRSS) on slip systems in quartz (e.g., Hobbs, 1985; Takeshita and Wenk, 1988; Mainprice and Nicolas, 1989). The most notable example is the mechanism switch from basal $\langle a \rangle$ to prism $[c]$ slip systems with increasing temperature in synthetic quartz documented by Griggs and Blacic (1965). Since both the basal $\langle a \rangle$ and prism $[c]$ slip systems accommodate the same shear strain component, ϵ_{XZ}, in the crystal coordinate system (Fig. 1), activation of only one family of slip systems between the two different families suffices to accommodate the shear strain component, ϵ_{XZ}. Therefore, the transition from basal $\langle a \rangle$ to prism $[c]$ slip systems is inevitable when prism $[c]$ slip becomes easier than basal $\langle a \rangle$ slip with increasing temperature. The mechanism switch from basal $\langle a \rangle$ to prism $[c]$ slip systems is perhaps associated with the intracrystalline water weakening of prism $[c]$ slip system which has been believed to be caused by the replacement of the strong Si–O bonding by weak hydrogen bonding (Si–OH · HO–Si) (Griggs and Blacic, 1965). Because the diffusion of water becomes enhanced with increasing temperature, and because prism $[c]$ would be more susceptible to intracrystalline water weakening than basal $\langle a \rangle$ slip systems, the mechanism switch can occur with increasing temperature.

The mechanism switch from basal $\langle a \rangle$ to prism $[c]$ slip systems has important consequences for the development of crystallographic preferred orientation during the plastic deformation of quartzite. This is due to the completely different lattice (external) rotation caused by the two different families of slip systems. Lister (1981) documented that simulated c-axis fabrics change from girdle pattern to X-maximum pattern (where the c-axes are dominantly aligned parallel to the maximum elongation direction) as the dominant slip direction changes from $\langle a \rangle$ to $[c]$. Many natural quartz c-axis fabrics reported to date show that slip in the $\langle a \rangle$ direction on cozonal glide planes is dominant in naturally deformed quartz at low–medium temperature (ca. 250–500°C) conditions (e.g., Bouchez and Pêcher, 1981). However, X-maximum fabric patterns in natural quartz have been found in naturally deformed granitic rocks deformed at a very high temperature close to the subsolidus temperature of granite (ca. 650–750°C) (e.g., Bouchez et al., 1984; Blumenfeld et al., 1986; Gapais and Barbarin, 1986; Mainprice et al., 1986; Garbutt and Teyssier, 1991). These observations clearly indicate that the basal-prism mechanism switch occurs at high temperatures in naturally deformed quartz.

In this paper, the deformation microstructures and quartz c-axis fabrics of seven metachert samples are documented. These samples consist of non-folded metacherts from the medium- to high-grade metamorphic zones of the Ryoke metamorphic belt in the Yanai district, southwestern Japan (Fig. 2). Furthermore, dislocation microstructures have been documented with transmission electron microscopy (TEM), in order to elucidate the operative slip direction (i.e., Burgers vector). By correlating the change in quartz fabric with petrologically based estimates of metamorphic conditions (Okudaira et al., 1993),

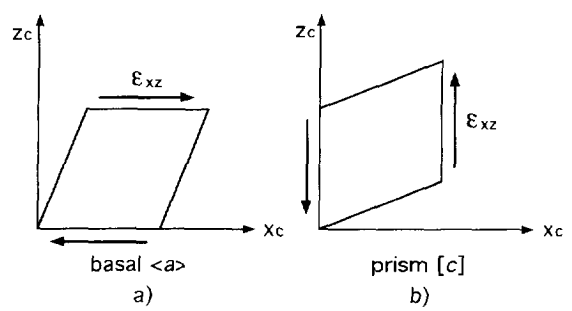

Fig. 1. Schematic illustration showing the basal $\langle a \rangle$ and prism $[c]$ slip systems in quartz, which accommodate the same shear strain component ϵ_{XZ} in the crystal coordinates. The Xc- and Zc-axes are chosen so that they coincide with the a-axis ($\langle 11\bar{2}0 \rangle$) and c-axis ([0001]), respectively.

the temperature at which the transition from basal ⟨a⟩ to prism [c] occurs is documented. The results obtained here could be used as a standard to infer the temperature condition for the mechanism switch from basal ⟨a⟩ to prism [c] slip systems based on the patterns of quartz c-axis fabric, and then they give

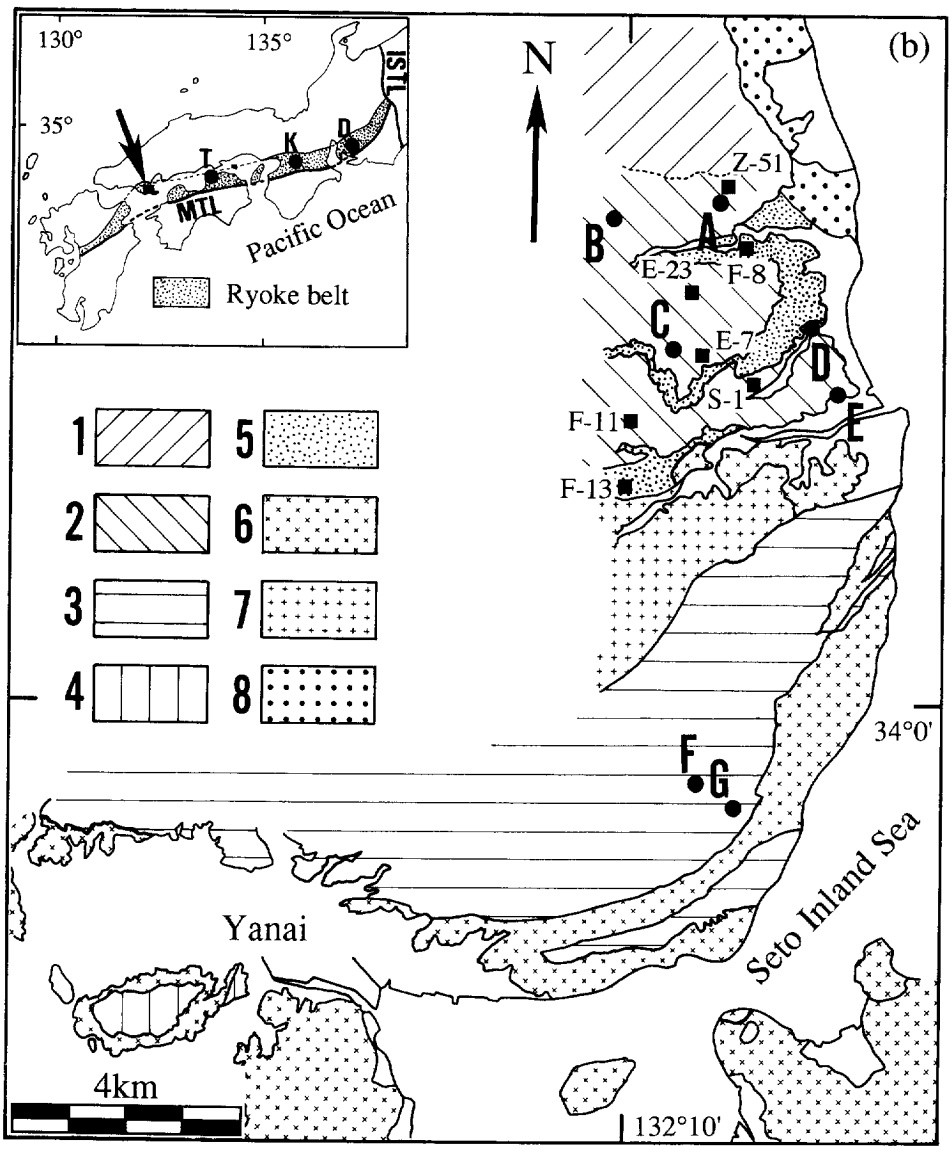

Fig. 2. Geological map of the Ryoke metamorphic belt in the Yanai district (simplified from Okudaira et al., 1993). (a) Index map of the investigated area. *MTL* = Median Tectonic Line. *ISTL* = Itoigawa–Shizuoka Tectonic Line; *D* = Dando district; *K* = Kasagi district; *T* = Teshima district. (b) Geological and metamorphic zonation map. *1–4* = Ryoke metamorphic rocks (*1* = biotite zone, *2* = cordierite zone; *3* = garnet zone, *4* = sillimanite zone); *5* = migmatite zone; *6* and *7* = Ryoke granites (*6* = older granites, *7* = younger granites). *8* = Hiroshima granites. The locations of samples for both petrological and microstructural analyses are shown by ■ and ●, respectively. ● with letters indicate localities of samples *A*, *B*, *C*, *D*, *E*, *F* and *G* for microstructural analyses. ■ indicate localities of samples for petrological analyses of metamorphic temperatures.

structural geologists another tool with which to estimate the temperature of deformation.

2. Geological setting

The Ryoke metamorphic belt in southwestern Japan (Fig. 2a), which consists of a large amount of granitoids and associated metamorphic rocks, is one of the typical low-pressure type metamorphic belts in the world (e.g., Miyashiro, 1961). The low-pressure type Ryoke metamorphic belt is truncated by the Median Tectonic Line (MTL) at the southern end, and juxtaposed to the high-pressure type Sambagawa metamorphic belt. Both the metamorphic belts, known as a paired metamorphic belt (Miyashiro, 1961), are Jurassic–Cretaceous in age (cf. Banno and Nakajima, 1992).

The Yanai district, southwestern Japan is mainly underlain by the low-pressure type Ryoke metamorphic rocks, the Ryoke granites which are divided into older and younger granites, and the Hiroshima granites (Fig. 2b; cf. Higashimoto et al., 1983; Okudaira et al., 1993; Ikeda, 1993). The Ryoke metamorphic rocks were mainly derived from pelites, psammites and cherts with subordinate amounts of calcareous and basic rocks, which presumably belong to a Jurassic accretionary complex (the Kuga Group) (cf. Higashimoto et al., 1983). They can be divided into the biotite, cordierite, sillimanite and garnet zones with increasing metamorphic grade in terms of the mineral assemblages in metapelites (Okudaira et al., 1993). In this district the biotite, cordierite, garnet and sillimanite zones are distributed from north to south (Fig. 2b). The distribution of the metamorphic zones results from the formation of nappes (Okudaira et al., 1993).

The granitic and metamorphic rocks in this district suffered two different phases of deformation (Okudaira et al., 1993); the earlier and later phases are called D_1 and D_2, respectively. During D_1, a distinct foliation parallel to lithologic layering was formed under the peak metamorphic conditions. D_2, which is not discussed here, is defined by the formation of nappes.

Matrix-forming minerals in metapelites, which were crystallized under the peak metamorphic conditions during D_1, have been analyzed to estimate the temperature conditions for the peak metamorphism. The peak metamorphic temperatures for the cordierite, sillimanite and garnet zones were estimated to be ca. 460–590, 630–690 and 730–7710°C, respectively (Okudaira et al., 1993). In the cordierite zone, where the basal-prism mechanism switch presumably occurs, quartz, plagioclase, K-feldspar, biotite, muscovite, cordierite and andalusite are stable in metapelites, and the metamorphic temperatures of the zone can be calculated by using the two-feldspar geothermometers (see Appendix A; Stormer, 1975; Stormer and Whitney, 1977; Haselton et al., 1983). The estimated temperatures are illustrated in Table 1.

Table 1
Metamorphic temperature estimates (°C) of pelitic rocks in the cordierite zone

Sample	X_{Na}^{Pl}	X_{Ca}^{Pl}	X_{Na}^{Kfs}	X_{K}^{Kfs}	Temperature (°C)		
					T_1	T_2	T_3
Z-51	0.743	0.249	0.090	0.909	445	490	425
F-8	0.749	0.236	0.133	0.865	503	553	501
E-23	0.732	0.258	0.120	0.878	491	539	485
E-7	0.737	0.251	0.156	0.842	535	589	546
S-1	0.807	0.183	0.161	0.830	517	573	509
F-11	0.610	0.379	0.142	0.856	566	616	589
F-13	0.759	0.231	0.179	0.820	552	612	569

Calibrations by the two-feldspar geothermometers (pressure = 3.0 kbar).
T_1 = Stormer (1975); T_2 = Stormer and Whitney (1977); T_3 = Haselton et al. (1983).
X_B^A represents molar fraction of component B in mineral A.

3. Sample description

The microstructures and *c*-axis fabrics of quartz grains in five metacherts (A, B C, D and E) from the cordierite zone and those in two samples (F and G) from the garnet zone are examined here. Localities of the seven investigated samples are indicated in Fig. 2b. In addition, in Fig. 3, a schematic cross section of the cordierite zone is presented to show the spatial relationship between the samples used for microstructural analyses and those used for metamorphic temperature analyses. An inset diagram in Fig. 3 illustrates the temperature variation in the cordierite zone which grades into the biotite zone to the north, and the garnet zone to the south. The geological structure of the cordierite zone is characterized by a monocline gently dipping toward the north with an open antiform north of the E–W-trending Tsuzu fault described by Higashimoto et al. (1983). Across the Tsuzu fault a structural discontinuity is observed, and in fact, the migmatite zone distributed south of the Tsuzu fault is truncated by the fault. Furthermore, the metamorphic temperature estimated for the sample Z-51 located north of the fault is significantly lower than those estimated for the samples located south of the fault. In the southern block, the temperatures of samples F-8 and E-23 are slightly lower than those of samples E-7, S-1, F-11, and F-13 (Fig. 3). Overall, the metamorphic temperatures increase from north to south with increasing structural level.

Samples A and B in the northern block were collected from nearly the same structural position in the uppermost part of the cordierite zone close to the cordierite isograd, and sample E in the southern block was collected from the lowermost part of the cordierite zone (Fig. 3). Samples C and D in the southern block were collected from structural positions ca. 500 and 200 m above that of sample E, respectively (Fig. 3). Although the metachert samples are taken from different structural levels, distribution of the metacherts in the cordierite zone is not sufficient to draw a fabric "isograd" similar to the case in the Saxony granulite terrain (see Lister and Dornsiepen, 1982). Samples F and G were collected from the garnet zone at similar structural positions.

These seven metacherts are characterized by a single foliation formed during the D_1 phase, which is defined either by the alternation of mica-rich and mica-poor layers or by the preferred shape orientation of mica grains. Since the D_2 phase deformation was localized at narrow zones and the metacherts examined show no evidence of D_2-folding both in outcrop and thin section scales, the amount of strain suffered during the D_2 phase could be neglected.

3.1. Deformation microstructures

Samples A and B consist of many small polygonal and few large recrystallized grains of quartz (Fig. 4a). The mean grain sizes of small polygonal grains

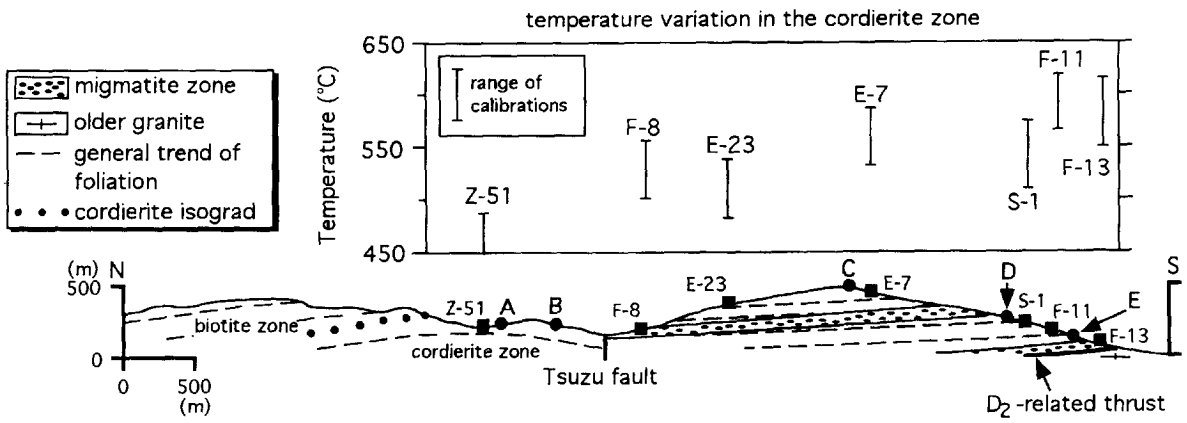

Fig. 3. Schematic cross section across the cordierite zone from north to south (Okudaira et al., 1993). ● and ■ indicate the structural positions of samples for microstructural analyses and for petrological analyses of metamorphic temperature, respectively. An inset diagram shows the metamorphic temperature variation in the cordierite zone.

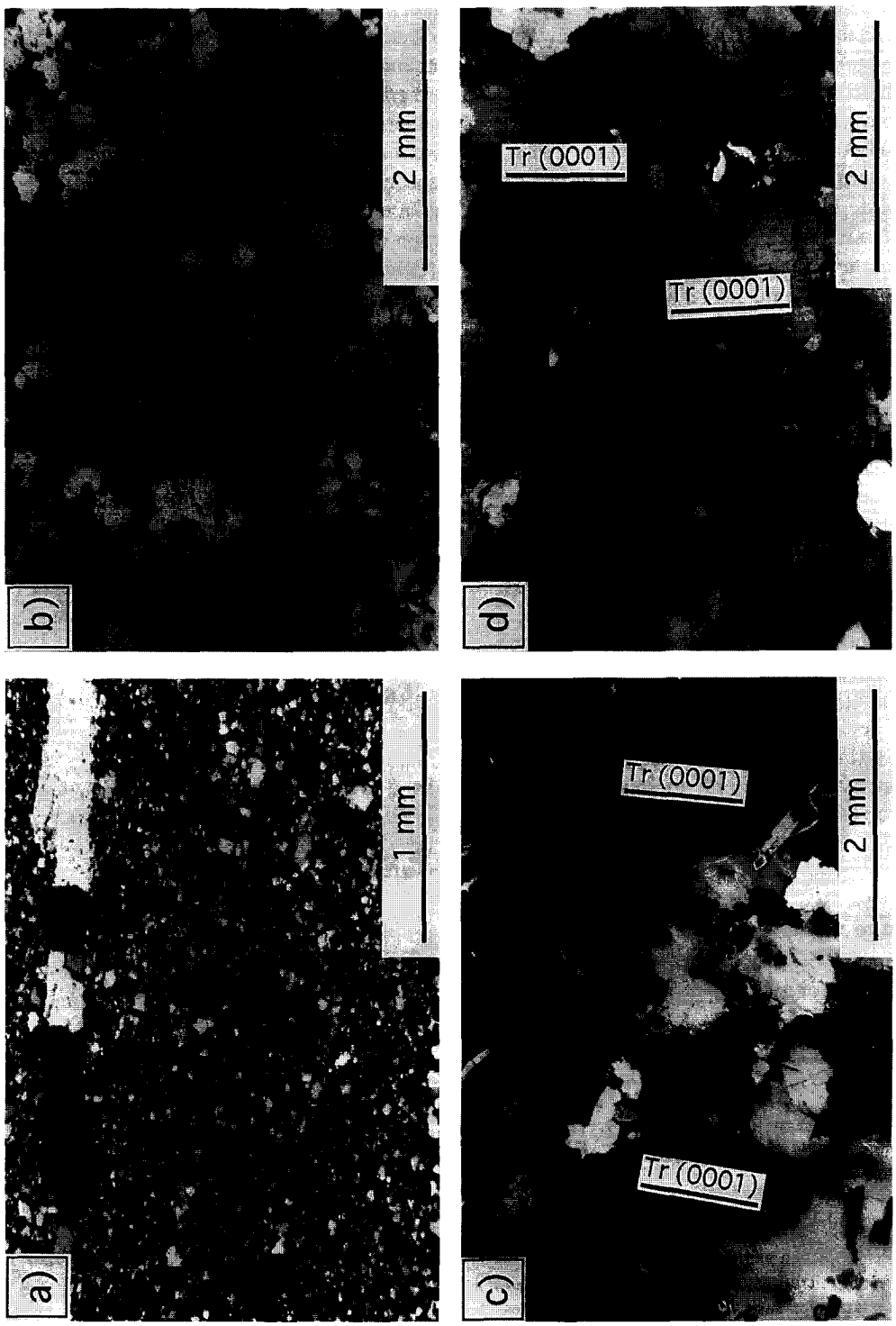

Fig. 4. Optical microstructures of quartz grains in the metacharts. (a) Sample A. (b) Sample C. (c) Sample D. (d) Sample IG. *Tr (0001)* denotes the trace of the basal plane in the quartz.

are ca. 40 μm (minimum 15 μm; maximum 65 μm) and 45 μm (minimum 12 μm; maximum 80 μm), whereas those of large grains are ca. 250 μm (minimum 145 μm; maximum 465 μm) and 145 μm (minimum 90 μm; maximum 275 μm) in samples A and B, respectively. In samples A and B, the large grains (open squares in Fig. 5a) are more elongated than the small grains (closed squares in Fig. 5a). Because the larger quartz grains exclusively form veinlets in samples A and B (Fig. 4a), it could be considered that these grains did not suffer significant grain size reduction by dynamic recrystallization after vein formation. Sample C shows a weak bimodal grain size distribution (Fig. 4b). The mean grain size of the smaller grains is ca. 250 μm (minimum 75 μm; maximum 540 μm), and that of the larger grains is ca. 1100 μm (minimum 700 μm; maximum 2480 μm).

Samples D, E, F and G exhibit essentially the same microstructure (Fig. 4c and d). These samples are mainly composed of large recrystallized grains (mainly ca. 200–3700 μm). The mean grain sizes of samples D, E, F and G are ca. 810 μm (minimum 60 μm; maximum 3600 μm), 880 μm (minimum 210 μm; maximum 2300 μm), 1450 μm (minimum 260 μm; maximum 4000 μm), and 1060 μm (minimum 140 μm; maximum 4150 μm), respectively, although the grain size varies considerably within one thin section for all the samples.

In summary, in the cordierite zone, the mean recrystallized grain size of quartz increases greatly from sample A (ca. 40 μm) to sample E (ca. 880 μm) with increasing structural level. Particularly, the abrupt increase in recrystallized grain size from sample B (45 μm) through C (250 μm) to D (810 μm) occurs within the structural distance less than 500 m. Here, the vertical displacement along the Tsuzu fault is assumed to be small. Because the increase in recrystallized quartz grain size is consistent with the rise of the petrologically estimated peak metamor-

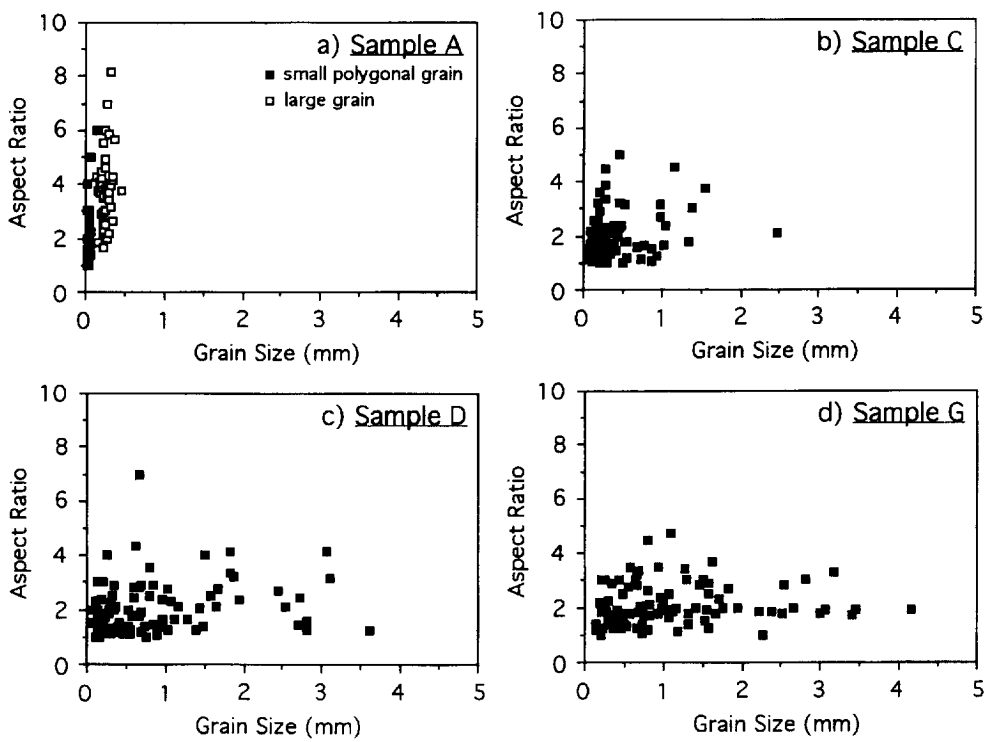

Fig. 5. Grain size (geometric mean of the length of long axis and that of short axis of quartz) versus aspect ratio (ratio of the length of long axis to that of short axis of quartz). □ = small grain; ■ = large grain. (a) Sample A, (b) Sample C. (c) Sample D. (d) Sample G.

phic temperatures (see upper inset diagram in Fig. 3), it is concluded that the deformation temperature increases from samples A and B through C to D and E.

The aspect ratio (ratio of long axis to short axis) versus grain size (geometric mean of long axis and short axis) of quartz grains in samples A, C, D and G is indicated in Fig. 5. The major difference between sample A and samples D and G is that for the former sample the aspect ratio varies greatly from 1 to 6 at a fairly constant grain size, and for the latter samples the grain size varies greatly at a fairly small aspect ratio (around 2). Sample C is intermediate between the two. The results overall represent a decrease of aspect ratio and an increase of grain size with increasing temperature.

The grain boundaries of the recrystallized quartz grains for all the samples, particularly samples C through G composed of larger grain sizes (> 250 μm), exhibit a cuspate shape indicative of grain boundary migration.

3.2. Quartz c-axis fabrics

The c-axis orientation of individual grains with respect to the structural reference frame (X—parallel to the lineation, Z—normal to the foliation, and Y—perpendicular to the X and Z directions) was determined using a universal stage. The lower hemisphere equal-area projections of quartz c-axis fabrics in the samples from the cordierite zone are illustrated in Fig. 6. Quartz c-axis fabrics in samples A and B, from a low-temperature part of the zone, show a type-II crossed girdle pattern (e.g., Lister, 1977; Price, 1985) with a half opening angle of 30–35°C (Fig. 6a and b), with a Y-submaximum for sample B. The c-axis fabric pattern in sample C shows a small-circle girdle around Z with the same half opening angle as those of samples A and B (Fig. 6c). In contrast, quartz c-axis fabrics in samples D and E from a high-temperature part of the zone have a distinct X-maximum which is rotated clockwise by 10–20° about Y from X. In addition, both the quartz

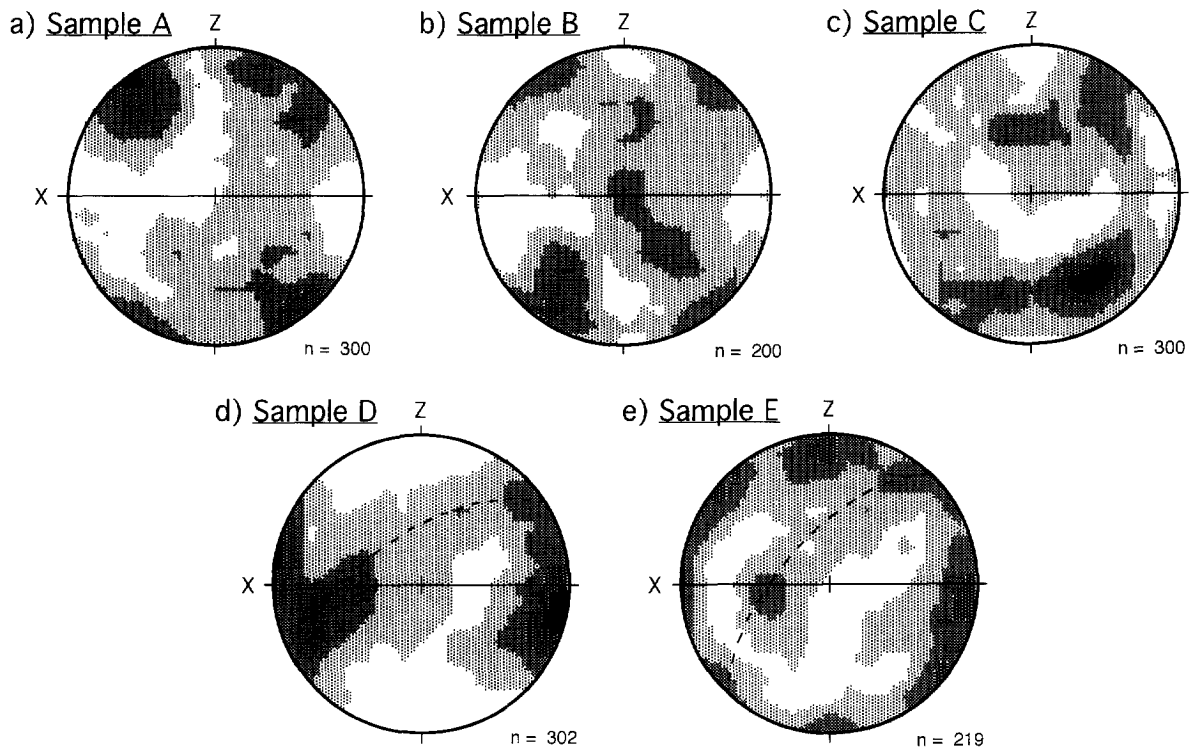

Fig. 6. Quartz c-axis fabrics from cordierite zone metacherts in the Yanai district, Ryoke metamorphic belt. (a) Sample A, 300 c-axes. (b) Sample B, 200 c-axes. (c) Sample C, 300 c-axes. (d) Sample D, 302 c-axes. (e) Sample E, 219 c-axes. Straight line shows a foliation (XY plane) defined by preferred shape orientation of mica grains. Kamb contours (2σ contour interval).

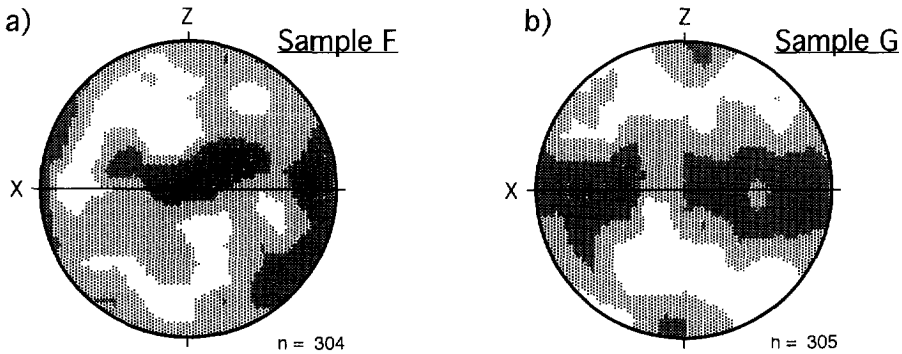

Fig. 7. Quartz *c*-axis fabrics from garnet zone metacherts in the Yanai district, Ryoke metamorphic belt. (a) Sample F, 304 *c*-axes. (b) Sample G, 305 *c*-axes. Equal area, lower hemisphere projection on *XZ* plane. Straight line shows a foliation (*XY* plane) defined by preferred shape orientation of mica grains. Kamb contours (2σ contour interval).

c-axis fabrics exhibit a faint great-circle girdle inclined at 45° to *Z*, and nearly parallel to *Y*, indicated by dashed lines in Fig. 6d and e. In sample E, a *Z*-maximum is apparent in addition to the above fabric components.

Quartz *c*-axis fabrics in samples from the garnet zone are illustrated in Fig. 7. The pattern in sample F shows a *Y*-maximum and an *X*-maximum (Fig. 7a). Sample G exhibits an *X*-maximum elongated toward *Y*, and a submaximum at *Z* (Fig. 7b).

3.3. Subgrain boundaries (SGBs)

During crystal plastic deformation by a combination of glide and climb, arrays of dislocations form SGBs to reduce stored elastic strain energy (Ball and Hirsch, 1955). Given that SGBs are lower-energy structures than free dislocations, they should be less susceptible to modification by post-deformation annealing (Mainprice et al., 1986). Therefore, SGBs in quartz are a useful indicator of the operative slip systems during high-temperature plastic deformation.

Quartz grains in samples A, B and C show little undulatory extinction, and have straight or slightly curved grain boundaries (Fig. 4a and b). In these samples, SGBs are rare and mostly parallel to the *c*-axes indicating that the SGBs are in the same zone as that of prismatic planes. In contrast, in samples D, E, F and G, SGBs are well developed and are irregularly curved or cuspate (Fig. 4c and d). In these samples the quartz *c*-axes are often preferentially oriented parallel to the lineation (Figs. 6 and 7), and most of the SGBs in such oriented quartz grains are nearly perpendicular to the *c*-axes. These observations indicate that the SGBs are subparallel to the basal (0001) plane. Such basal SGBs often form approximately square subgrains with subordinate planar prismatic SGBs (Fig. 4c and d).

A statistical analysis of the angles between SGBs and [*c*] axes in the grains containing SGBs was undertaken for samples exhibiting many visible SGBs (Fig. 8). In the cordierite zone, samples B and C show a high population of prismatic SGBs (Fig. 8a and b). In contrast, in samples D and E, about 20% of the SGBs are in a prismatic orientation, while more than 60% are in basal to sub-basal orientations (Fig. 8c and d). In the garnet zone, more than 80% of the SGBs are in basal to sub-basal orientations for sample F (Fig. 8e), whereas the population is almost entirely represented by basal SGBs for sample G (Fig. 8f).

3.4. TEM observations

Direct observation of dislocations by TEM has been conducted to determine the slip systems operative in deformed quartz (e.g., Nicolas and Poirier, 1976). To confirm our understanding of the operative slip systems which can be independently derived from the pattern of quartz *c*-axis fabric and orientation of SGBs, TEM observations were made of

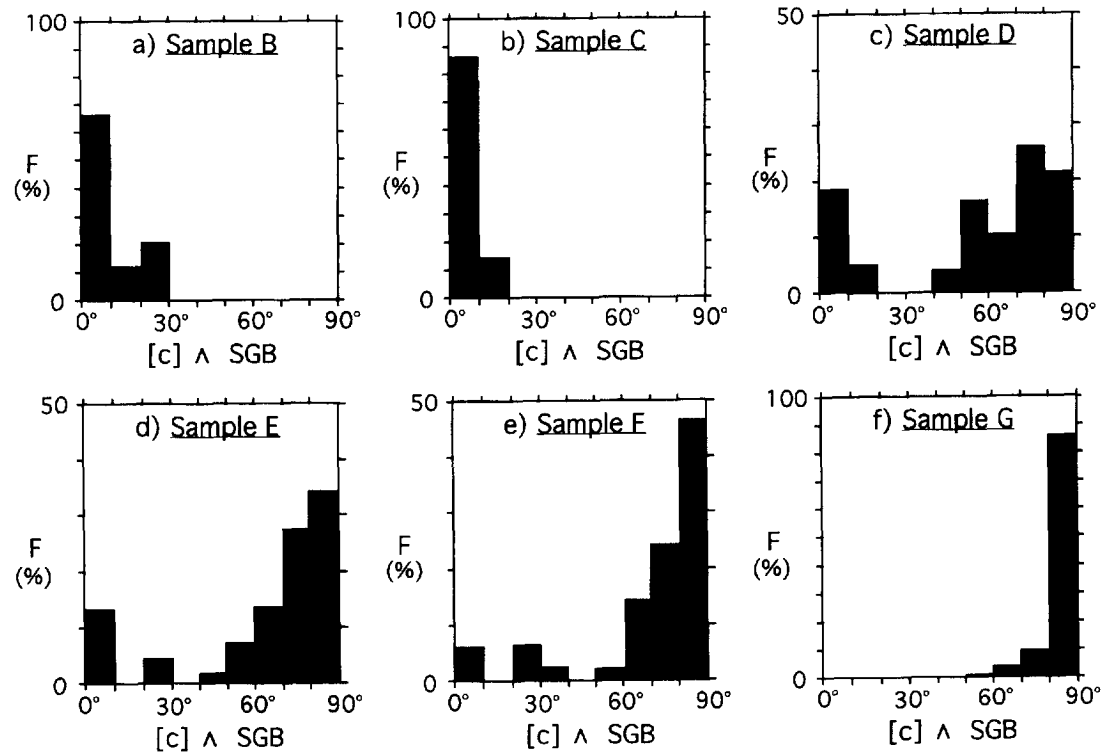

Fig. 8. Histogram of the angles between subgrain boundaries and *c*-axes in subgrains. (a) Sample B. (b) Sample C. (c) Sample D. (d) Sample E. (e) Sample F. (f) Sample G.

samples A, D and G. Following optical studies, individual quartz grains containing well-defined SGBs were selected. All observations were carried out with a JEOL JEM-200CX transmission electron microscope at Ehime University using an accelerating voltage of 200 kV. The samples were ion thinned and carbon coated for the TEM observation.

Observations were made on free dislocations and SGBs in the samples. In addition, free dislocation densities were determined. For the determination of dislocation density, the number of free dislocations within ca. five areas ranging from about 5.3×3.8 to 3.1×2.2 μm^2 was counted for each grain. Some typical images of dislocation microstructures are shown in Fig. 9. In sample A dislocations are fairly homogeneously distributed (Fig. 9a), while in sample G many dislocation loops are observed in addition to curved free dislocations (Fig. 9b). The free dislocation densities (ρ) in samples A and G are similar, which are $\rho = (8.9 \pm 1.4) \times 10^8$ cm^{-2} and $\rho = (1.3 \pm 0.4) \times 10^9$ cm^{-2}, respectively. In sample D many subgrain boundaries are observed, which are composed of either simple arrays of parallel dislocations or networks of dislocations often curved. Most of the subgrain boundaries are nearly normal to *c* [0001] direction (Fig. 9c). In samples A and G many bubbles are observed (Fig. 9a and b). The bubbles give rise to such contrast as a pair of lobes symmetrically placed about a line of no contrast under TEM (cf. McLaren, 1991). The line of no contrast is often parallel to [0001] in sample G.

Analysis of operative slip systems was carried out using the standard technique of "invisibility criteria", which has been shown to be effective in quartz (e.g., Hirsch et al., 1965; Ardell et al., 1974). For a dislocation to be invisible, the following condition is required, namely the vector products $\mathbf{g} \cdot \mathbf{b} = 0$ for a pure screw dislocation, and $\mathbf{g} \cdot \mathbf{b} \times \mathbf{u} = 0$ for a

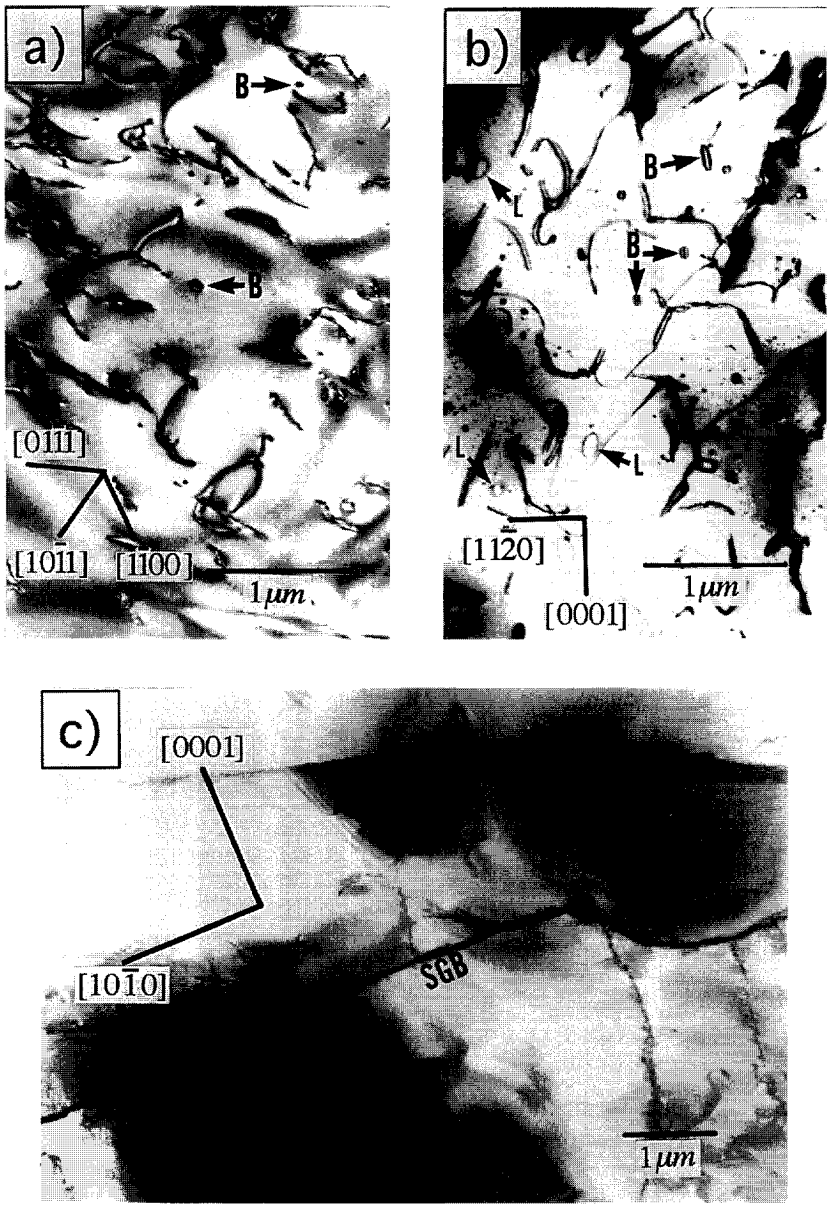

Fig. 9. TEM bright-field micrographs of the deformed quartz from samples A, D and G. (a) Sample A. (b) Sample D. (c) Sample G. Bubbles, dislocation loops, and subgrain boundaries are marked by *B*, *L* and *SGB*, respectively.

pure edge dislocation, where **g** is the diffracting vector, **b** the Burgers vector and **u** the unit vector along the dislocation line. Bright and dark field images of a free dislocation under TEM in the quartz from sample G are shown in Fig. 10a and b, respectively. Since the dislocation is almost out of contrast in the dark field image using the diffraction **g** = [11$\bar{2}$0], and since the dislocation line is nearly paral-

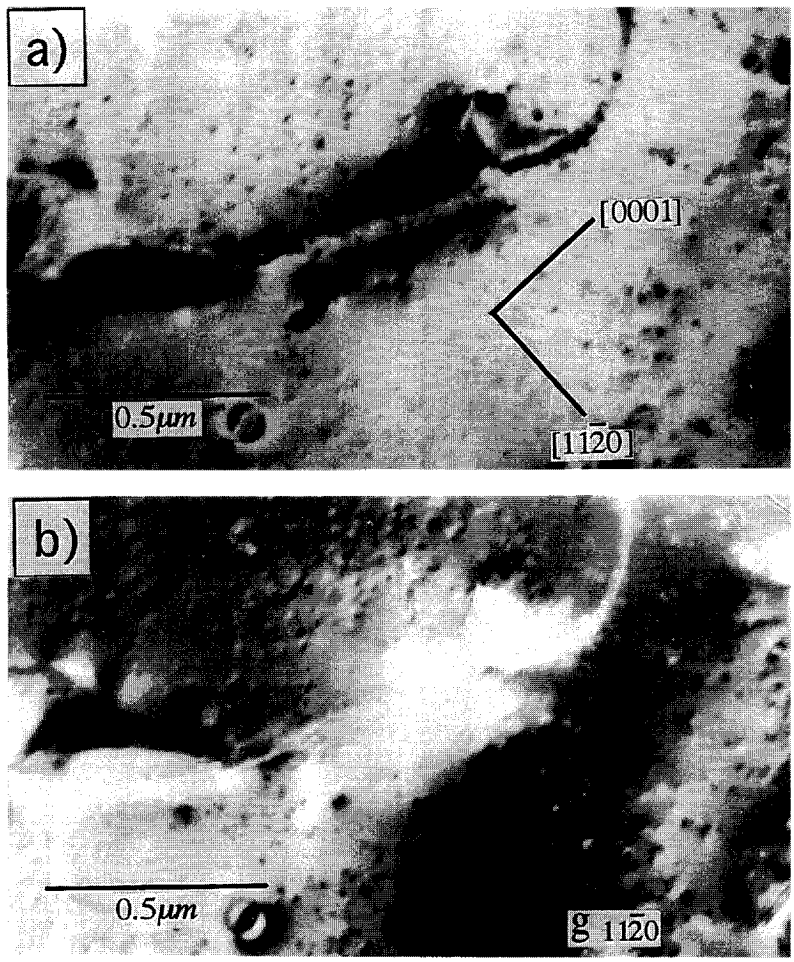

Fig. 10. TEM micrographs of deformed quartz from sample G. (a) A bright-field image of free dislocation. (b) A dark-field image of the same area. Diffracting vector $\mathbf{g} = [11\bar{2}0]$.

lel to [0001], the dislocation must be identified as a screw dislocation with the Burgers vector of [0001].

4. Discussion

4.1. Inferred slip systems

Dominant slip systems in quartz polycrystals can be estimated from the pattern of *c*-axis fabrics and preferred maximum orientations (e.g., Lister et al., 1978; Lister and Hobbs, 1980). Moreover, the angle between the *c*-axis and SGBs in a quartz grain allows us to infer the operative slip system (e.g., Christie and Green, 1964; Trépied et al., 1980; Blumenfeld et al., 1986; Mainprice et al., 1986).

The *c*-axis fabrics in samples A and B show type-II crossed girdle patterns (Fig. 6a and b) with a half opening angle of 30–35°, and a *Y*-submaximum is present in sample B. The *c*-axis fabric pattern in sample C shows a small-circle girdle around *Z* with the same half opening angle (Fig. 6c). The type-II crossed girdle and small circle pattern with large half opening angles can be produced by the dominant activation of basal $\langle a \rangle$ and prism $\langle a \rangle$ slip systems (Lister and Hobbs, 1980; Takeshita and Wenk, 1988; Wenk et al., 1989).

In sample F the pattern of *c*-axis fabric shows a

Y-maximum and an X-maximum (Fig. 7a). The fabric pattern in sample G is characterized by an X-maximum elongated toward Y (Fig. 7b). A high concentration of c-axes near X has probably been produced by the dominant activation of the prism [c] slip system, since numerical simulation indicates that X-maximum c-axis fabrics are produced by the dominant activity of prism [c] (Lister, 1981). Evidence for prism [c] slip has previously been documented in natural quartz aggregates exhibiting X-maximum c-axis fabrics deformed at temperatures close to granite subsolidus (Blumenfeld et al., 1986; Mainprice et al., 1986). The high concentration of c-axes near Y has probably been produced by the activation of prism $\langle a \rangle$ slip systems (Wenk et al., 1989). Consequently, the fabric patterns in samples F and G are concluded to have been produced by the dominant activation of prism [c] slip system, with a subordinate activation of prism $\langle a \rangle$ slip.

The c-axis fabric patterns in samples D and E are characterized by a distinct X-maximum and a faint great-circle girdle inclined $\sim 45°$ to Z and nearly parallel to Y. These fabric patterns can be interpreted as a transitional between a type-II crossed girdle and an X-maximum. Therefore, the c-axis fabric patterns illustrate simultaneous operation of prism [c], prism $\langle a \rangle$ and basal $\langle a \rangle$ slip systems (cf. Lister, 1981).

We currently do not have a good explanation for a maximum at Z observed for samples E and G. The maximum could be associated with the grain growth during deformation (e.g., Gleason et al., 1993).

The presence of basal SGBs in deformed quartz is exclusively characteristic of [c] slip, whereas the presence of prismatic SGBs indicates the operation of $\langle a \rangle$ slip (e.g., Christie and Green, 1964; Trépied et al., 1980; Blumenfeld et al., 1986; Mainprice et al., 1986). The high frequency of prismatic SGBs in the quartz from samples A, B and C indicates that the slip direction is dominantly in $\langle a \rangle$ (see Fig. 8a and b). In contrast, the dominance of basal SGBs in the quartz from samples D, E, F and G indicates that [c] slip dominates over $\langle a \rangle$ slip in these samples (see Fig. 8c, d, e and f). However, $\langle a \rangle$ slip indicated by prismatic SGBs (i.e. [c] $\wedge$ SGB $\cong 0°$) still operated in samples D and E, while the activity of $\langle a \rangle$ slip is negligible in samples F and G. Although the angle between SGBs and c-axes in grains containing SGBs should be 90° for [c] slip, the observed angles are distributed over a wide range for samples D, E and F (Fig. 8). These basal SGBs are rarely planar and sometimes exhibit a cuspate shape under optical (Fig. 4c and d) and electron microscopic (Fig. 9c) observation. The curved and cuspate basal SGBs are probably caused by subgrain boundary migration during syn- and/or post-dynamic recrystallization (cf. Urai et al., 1986). Therefore, the sub-basal subgrain boundaries, that is [c] $\wedge$ SGB = 60–80°, could be attributed to the migration of basal SGBs.

TEM observations on quartz grains from sample G reveals the presence of free dislocations with the [0001] Burgers vector (Fig. 10), and observations in the quartz from sample D show the frequent occurrence of basal subgrain boundaries (Fig. 9c). These observations are consistent with the other observations indicating the dominant activation of prism [c] slip in samples D and G.

In summary, based on the pattern of c-axis fabrics, orientation of SGBs, and Burgers vector analysis, it has been shown that samples A, B and C were deformed by the dominant activation of basal $\langle a \rangle$ and prism $\langle a \rangle$ slip systems, whereas samples F and G were deformed by the dominant activation of prism [c] slip systems, with subordinate activation of prism $\langle a \rangle$ slip system. Although [c] slip is dominant in samples D and E, the activation of slip systems is characterized by a transitional regime where basal $\langle a \rangle$, prism $\langle a \rangle$ and prism [c] slip systems all operated. In conclusion, the basal-prism mechanism switch in the deformed quartz occurred between samples A, B and C and samples D and E, although the activity of basal $\langle a \rangle$ slip systems is not completely replaced by that of prism [c] slip systems in samples D and E.

4.2. Transition conditions from basal $\langle a \rangle$ to prism [c] slip

Quartz c-axis fabrics have been investigated elsewhere in the Ryoke metamorphic belt (e.g., Nureki, 1960; Hara, 1962). In the Kasagi district (Fig. 2a), Hara (1962) suggested that quartz c-axis fabrics characterized by a crossed girdle with a distinct Y-maximum were developed at temperatures higher than ca. 450°C. The fabric patterns suggest that the prism $\langle a \rangle$ and basal $\langle a \rangle$ slip systems were active.

The results presented in this paper show that the mechanism switch from basal $\langle a \rangle$ to prism [c] slip

systems occurs between samples A, B and C and samples D and E from naturally deformed metacherts in the Ryoke metamorphic belt, even though these two groups of samples occur only ca. 400 m apart in structural level and coexist in the same metamorphic grade. In samples F and G from the garnet zone, [c] slip exclusively operates. The temperatures in the cordierite zone in which samples A through E belong are estimated to be in the range from 460 to 590°C by two-feldspar geothermometers (Table 1; Fig. 3). More precisely, the metacherts deformed at ca. 460–550°C (samples A, B and C) show no evidence of prism [c] slip, those deformed at ca. 550–590°C (samples D and E) show about 75–80% [c] slip, and those from the garnet zone (samples F and G) show $\cong$ 100% prism [c] slip (see Fig. 8). Therefore, we can conclude that the basal-prism mechanism switch probably occurred within the temperature range of 550–600°C.

The *X*-maximum *c*-axis fabric patterns in naturally deformed quartz have been reported to date in rocks deformed under very high temperatures close to the granite subsolidus (e.g., Bouchez et al., 1984; Blumenfeld et al., 1986; Gapais and Barbarin, 1986; Mainprice et al., 1986; Garbutt and Teyssier, 1991). Mainprice et al. (1986) also observed the *X*-maximum *c*-axis fabrics indicative of dominant prism [c] slip in migmatites and granitic veins deformed at 650–750°C. Therefore, the temperature condition of 550–600°C estimated in this study for the basal-prism mechanism switch in quartz is somewhat lower than those inferred from the previous studies.

Mainprice et al. (1986) emphasized that the association of very high-temperature and wet or hydrous conditions appears to be the key requirement to activate [c] slip. It should be also noted that in synthetic quartz which contains abundant intracrystalline water (order of 0.1 wt%), [c] slip is preferred over ⟨a⟩ slip at relatively low temperatures (e.g., Griggs and Blacic, 1965; Linker et al., 1984). Because our metachert samples include many hydrous minerals such as biotite and muscovite and these minerals could have released a significant amount of water above 500°C by dehydration reactions (cf. Walther and Orville, 1982), it is conceivable that the abrupt increase of water content in rock with increasing temperature above ca. 500°C could have caused the increase in the activity of *c*-slip, and thus resulted in the basal-prism mechanism switch. This is partly evidenced by the presence of numerous bubbles in the deformed quartz revealed by TEM observations (Fig. 9a and b), while the concentration of bubbles mainly along dislocations suggests significant recovery at high temperature (e.g., Christie and Ardell, 1976; Drury, 1993). Furthermore, the abnormal increase of recrystallized quartz grain size with increasing temperature above ca. 550°C, which seems to be correlated with the mechanism switch from ⟨a⟩ to [c] slip, could have been accomplished by water-assisted grain boundary migration (growth) (e.g., Urai et al., 1986), although the abnormal increase of recrystallized grain size could have resulted from the fact that a critical temperature for grain boundaries to break away from the pinning effects of impurities was exceeded in the metachert samples (cf. Guillope and Poirier, 1979).

5. Conclusions

Quartz *c*-axis fabrics of naturally deformed quartz in metacherts from the Ryoke metamorphic belt in the Yanai district, southwestern Japan, suggest that the prism [c], prism ⟨a⟩ and basal ⟨a⟩ slip systems were activated during the plastic deformation under high-temperature metamorphic condition. Quartz *c*-axis fabric patterns change from girdle type, through *X*-maximum with faint crossed girdle, to *X*-maximum with increasing temperature. The dominant orientation of subgrain boundaries in the quartz also changes from prism to basal planes with increasing temperature, which is closely correlated with the quartz fabric change. The fabric transition is also accompanied by an abrupt increase of recrystallized quartz grain size. Moreover, TEM observations support the dominant activation of [c] slip through the presence of (0001) subgrain boundaries and free dislocations with the [0001] Burgers vector in the quartz from the metachert samples exhibiting an *X*-maximum *c*-axis fabric. Based on these observations it is concluded that the mechanism switch from basal ⟨a⟩ to prism [c] slip systems occurred with increasing temperature. The transition temperature is petrologically estimated to be ca. 550–600°C at the natural strain rate. Our estimated temperature for the basal-prism mechanism switch is significantly lower

than the temperature conditions for dominant c-slip reported in previous studies (ca. 650–750°C). However, the conditions for transition from basal $\langle a \rangle$ to prism $[c]$ have not previously been clearly established. Finally, we suggest that the transition from basal $\langle a \rangle$ to prism $[c]$ slip systems in naturally deformed quartz, which is reflected in the change in quartz c-axis fabric and orientation of SGBs, provides a good indicator of high-temperature deformation conditions in metamorphic tectonites.

Acknowledgements

We express our sincere thanks to N. Sakakibara, H.-R. Wenk, A. Kronenberg and A. McGrew for constructive comments on an early version of the manuscript and J. Tullis and an anonymous reviewer for constructive reviews. We also thank A. Minami at Hiroshima University for technical assistance of EPMA analysis.

Appendix A

Metamorphic temperatures of the cordierite zone calculated by using the two-feldspar geothermometers are given in Table 2, where T, P, X_{K}^{Kfs}, X_{Na}^{Kfs}, X_{Ca}^{Pl}, and X_{Na}^{Pl}, are temperature (°C), pressure (bar), molar fractions of potassium and sodium in K-feldspar, and molar fractions of calcium and sodium in plagioclase, respectively. Eqs. A-1, A-2 and A-3 are from Stormer (1975), Stormer and Whitney (1977) and Haselton et al. (1983), respectively. The metamorphic pressure of the cordierite zone has been estimated to be ca. 3 kbar (Okudaira et al., 1993), and the estimated temperatures are illustrated in Table 1.

References

Ardell, A.J., Christie, J.M. and McCormick, J.W., 1974. Dislocation images in quartz and the determination of Burgers vectors. Philos. Mag., 29: 1399–1411.

Ball, C.J. and Hirsch, P.B., 1955. Surface distribution of dislocations in metals. Philos. Mag., 46: 1343–1352.

Banno, S. and Nakajima, T., 1992. Metamorphic belts of Japanese Islands. Annu. Rev. Earth Planet. Sci., 20: 159–179.

Blumenfeld, P., Mainprice, D. and Bouchez, J.-L., 1986. C-slip in quartz from subsolidus deformed granite. Tectonophysics, 127: 97–115.

Bouchez, J.L. and Pêcher, A., 1981. The Himalayan Main Central Thrust pile and its quartz-rich tectonites in central Nepal. Tectonophysics, 78: 23–50.

Bouchez, J.-L., Mainprice, D.H., Trépied, L. and Doukhan, J.C., 1984. Secondary lineation in a high-T quartzite (Galicia, Spain): An explanation for an abnormal fabric. J. Struct. Geol., 6: 159–165.

Christie, J.M. and Ardell, A.J., 1976. Deformation structures in minerals. In: H.-R. Wenk (Editor), Electron Microscopy in Mineralogy. Springer-Verlag, New York, NY, pp. 374–403.

Christie, J.M. and Green, H.W., 1964. Several new slip mechanisms in quartz. EOS, 45: 103.

Drury, M.R., 1993. Deformation lamellae in metals and minerals. In: J.N. Boland and J.D. Fitz (Editors), Defects and Processes in the Solid State: Geoscience Application. Elsevier, Amsterdam, pp. 195–212.

Gapais, D. and Barbarin, B., 1986. Quartz fabric transition in a cooling syntectonic granite (Hermitage Massif, France). Tectonophysics, 125: 357–370.

Table 2

$$T(^{\circ}C) = \frac{6326.7 - 9963.2X_{Na}^{Kfs} + 943.3\left(X_{Na}^{Kfs}\right)^2 + 2690.2\left(X_{Na}^{Kfs}\right)^3 + \left[0.0925 - 0.1458X_{Na}^{Kfs} + 0.0141\left(X_{Na}^{Kfs}\right)^2 + 0.0392\left(X_{Na}^{Kfs}\right)^3\right]P}{-1.9872\ln\left(\frac{X_{Na}^{Kfs}}{X_{Na}^{Pl}}\right) + 4.6321 - 10.815X_{Na}^{Kfs} + 7.7345\left(X_{Na}^{Kfs}\right)^2 - 1.5512\left(X_{Na}^{Kfs}\right)^3} - 273 \quad \text{(A-1)}$$

$$T(^{\circ}C) = \frac{7973.1 - 16910.6X_{Na}^{Kfs} + 9901.9\left(X_{Na}^{Kfs}\right)^2 + \left[0.11 - 0.22X_{Na}^{Kfs} + 0.11\left(X_{Na}^{Kfs}\right)^2\right]P}{-1.9872\ln\left(\frac{X_{Na}^{Kfs}}{X_{Na}^{Pl}}\right) + 6.48 - 21.58X_{Na}^{Kfs} + 23.72\left(X_{Na}^{Kfs}\right)^2 - 8.62\left(X_{Na}^{Kfs}\right)^3} - 273 \quad \text{(A-2)}$$

$$T(^{\circ}C) = \frac{\left(X_{K}^{Kfs}\right)^2\left(18810 + 17030X_{Na}^{Kfs} + 0.364P\right) - \left(X_{Ca}^{Pl}\right)^2\left(28230 - 39520X_{Na}^{Pl}\right)}{10.3\left(X_{K}^{Kfs}\right)^2 + 8.3143\ln\left[\frac{\left(X_{Na}^{Pl}\right)^2\left(2 - X_{Na}^{Pl}\right)}{X_{Na}^{Kfs}}\right]} - 273 \quad \text{(A-3)}$$

Garbutt, J.M. and Teyssier, C., 1991. Prism ⟨c⟩ slip in the quartzites of the Oakhurst Mylonite Belt, California. J. Struct. Geol., 13: 657–666.

Gleason, G.C., Tullis, J. and Heidelbach, F., 1993. The role of dynamic recrystallization in the development of lattice preferred orientations in experimentally deformed quartz aggregates. J. Struct. Geol., 15: 1145–1168.

Griggs, D.T. and Blacic, J.D., 1965. Quartz: anomalous weakness of synthetic crystals. Science, 147: 292–295.

Guillope, M. and Poirier, J.P., 1979. Dynamic recrystallization during creep of single-crystalline halite: an experimental study. J. Geophys. Res., 84: 5557–5567.

Hara, I., 1962. Studies on the structure of the Ryoke metamorphic rocks of the Kasagi district, Southwest Japan. J. Sci. Hiroshima Univ., C4: 163–224.

Haselton, H.T., Hovis, G.L., Hemingway, B.S. and Robie, R.A., 1983. Calorimetric investigation of the excess entropy of mixing in analbite-sanidine solid solutions: lack of evidence for Na, K short-range order and implications for two-feldspar thermometry. Am. Mineral., 68: 398–413.

Higashimoto, S., Nureki, T., Hara, I., Tsukuda, E. and Nakajima, T., 1983. Geology of the Iwakuni district. Quadrangle series, scale 1 : 50,000. Geol. Surv. Japan, 79 pp. (in Japanese with English abstract).

Hirsch, P.B., Howie, A., Nicholson, R.B., Pashley, D.W. and Whelan, M.J., 1965. Electron Microscopy of Thin Crystals. Butterworths, London, 563 pp.

Hobbs, B.E., 1981. The influence of metamorphic environment upon the deformation of minerals. Tectonophysics, 78: 335–383.

Hobbs, B.E., 1984. Point defect chemistry of minerals under a hydrothermal environment. J. Geophys. Res., 89: 4026–4038.

Hobbs, B.E., 1985. The geological significance of microfabric analysis, In: H.-R. Wenk (Editor), Preferred Orientation in Deformed Metals and Rocks: An Introduction to Modern Texture Analysis. Academic Press, London, pp. 463–484.

Ikeda, T., 1993. Compositional zoning patterns of garnet during prograde metamorphism from the Yanai district, Ryoke metamorphic belt, southwest Japan. Lithos, 30: 109–121.

Kronenberg, A.K. and Tullis, J., 1984. Flow strengths of quartz aggregates: grain size and pressure effects due to hydrolytic weakening. J. Geophys. Res., 89: 4281–4297.

Law, R.D., Knipe, R.J. and Dayan, H., 1984. Strain path partitioning within thrust sheets: microstructural and petrofabric evidence from the Moine Thrust zone at Loch Eriboll, northwest Scotland. J. Struct. Geol., 6: 477–497.

Linker, M.F., Kirby, S.H., Ord, A. and Christie, J.M., 1984. Effects of compression direction on the plasticity and rheology of hydrolytically weakened synthetic quartz crystals at atmospheric pressure. J. Geophys. Res., 89: 4241–4255.

Lister, G.S., 1977. Crossed-girdle c-axis fabrics in quartzites plastically deformed by plane strain and progressive simple shear. Tectonophysics, 39: 51–54.

Lister, G.S., 1981. The effect of the basal-prism mechanism switch on fabric development during plastic deformation of quartzite. J. Struct. Geol., 3: 67–76.

Lister, G.S. and Dornsiepen, U.F., 1982. Fabric transitions in the Saxony granulite terrain. J. Struct. Geol., 4: 81–92.

Lister, G.S. and Hobbs, B.E., 1980. The simulation of fabric development during plastic deformation and its application to quartzite: the influence of deformation history. J. Struct. Geol., 2: 355–370.

Lister, G.S., Paterson, M.S. and Hobbs, B.E., 1978. The simulation of fabric development in plastic deformation and its application to quartzite: the model. Tectonophysics, 45: 107–158.

Mainprice, D. and Nicolas, A., 1989. Development of shape and lattice preferred orientations: application to the seismic anisotropy of the lower crust. J. Struct. Geol., 11: 175–189.

Mainprice, D., Bouchez, J.-L., Blumenfeld, P. and Tubiá, J.M., 1986. Dominant c slip in naturally deformed quartz: Implications for dramatic plastic softening at high temperature. Geology, 14: 819–822.

McLaren, A.C., 1991. Transmission Electron Microscopy of Minerals and Rocks. Cambridge Univ. Press, Cambridge, 387 pp.

Miyashiro, A., 1961. Evolution of metamorphic belts. J. Petrol., 2: 277–311.

Nicolas, A. and Poirier, J.P., 1976. Crystalline Plasticity and Solid State Flow in Metamorphic Rocks. Wiley, London, 444 pp.

Nureki, T., 1960. Structural investigation of the Ryoke metamorphic rocks of the area between Iwakuni and Yanai, Southwestern Japan. J. Sci. Hiroshima Univ., C3: 69–141.

Okudaira, T., Hara, I., Sakurai, Y. and Hayasaka, Y., 1993. Tectono-metamorphic processes of the Ryoke belt in the Iwakuni-Yanai district, southwest Japan. In: M. Komatsu, T. Takeshita and M. Sakakibara (Editors), Evolution of the Arc Crust in Southwest Japan. Mem. Geol. Soc. Jpn., 42: pp. 91–120.

Price, G.P., 1985. Preferred orientations in quartzites. In: H.-R. Wenk (Editor), Preferred Orientation in Deformed Metals and Rocks: An Introduction to Modern Texture Analysis. Academic Press, London, pp. 385–406.

Stormer, J.C., 1975. A practical two-feldspar geothermometer. Am. Mineral., 60: 667–674.

Stormer, J.C. and Whitney, J.A., 1977. Two-feldspar geothermometry in granulite facies metamorphic rocks. Contrib. Mineral. Petrol., 65: 123–133.

Takeshita, T. and Wenk, H.-R., 1988. Plastic anisotropy and geometrical hardening in quartzites. Tectonophysics, 149: 345–361.

Trépied, L., Doukhan, J.C. and Paquet, J., 1980. Subgrain boundaries in quartz: Theoretical analysis and microscopic observations. Phys. Chem. Metals, 5: 201–218.

Tullis, J., Christie, J.M. and Griggs, D.T., 1973. Microstructures and preferred orientations of experimentally deformed quartzites. Bull. Geol. Soc. Am., 84: 297–314.

Urai, J.L., Means, W.D. and Lister, G.S., 1986. Dynamic recrystallization in minerals. In: B.E. Hobbs and H.C. Heard (Editors), Mineral and Rock Deformation: Laboratory Studies. Am. Geophys. Union Geophys. Monogr., 36: 166–199.

Walther, J.V. and Orville, P.M., 1982. Volatile production and transport in regional metamorphism. Contrib. Mineral. Petrol., 79: 252–257.

Wenk, H.-R., Canova, G., Molinari, A. and Kocks, U.F., 1989. Viscoplastic modeling of texture development in quartzite. J. Geophys. Res., 94: 17,895–17,906.